Ceramics International 46 (2020) 14864–14871

Contents lists available at ScienceDirect

Ceramics International

journal homepage: www.elsevier.com/locate/ceramint

Stabilization of the γ-Ag_2WO_4 metastable pure phase by coprecipitation method using polyvinylpyrrolidone as surfactant: Photocatalytic property

N.F. Andrade Neto[a,*], J.M.P. Silva[a], R.L. Tranquilin[b], E. Longo[b], M.R.D. Bomio[a], F.V. Motta[a]

[a] LSQM, Laboratory of Chemical Synthesis of Materials, Department of Materials Engineering, Federal University of Rio Grande do Norte, UFRN, P.O. Box 1524, Natal, RN, Brazil

[b] CDMF-UFSCar, Universidade Federal de São Carlos, P.O. Box 676, São Carlos, SP, 13565-905, Brazil

ARTICLE INFO

Keywords:
Polyvinylpyrrolidone
Metastable phases
γ-Ag_2WO_4
β-Ag_2WO_4
Photocatalysis

ABSTRACT

In this work, the effect of polyvinylpyrrolidone (PVP) concentration as a surfactant was studied in the stabilization of the metastable phase γ-Ag_2WO_4 by the coprecipitation method at room temperature. The phases obtained were characterized by X-ray diffraction (XRD), Raman spectroscopy, scanning electron microscopy (SEM), transmission electron microscopy (TEM) and spectroscopy in the ultraviolet–visible region (UV–Vis). The photocatalytic activity was estimated by varying the concentration of methylene blue dye. The diffractograms indicate that 0.3 g of PVP is ideal for obtaining the single phase of γ-Ag_2WO_4, as larger or smaller amounts favor the appearance of β-Ag_2WO_4 as a secondary phase while the absence of PVP formed the α-Ag_2WO_4 phase. UV–Vis spectroscopy showed that both phases have absorption in the ultraviolet region, where the γ-Ag_2WO_4 phase has a higher absorption at shorter wavelengths. The micrographs indicate that the β-Ag_2WO_4 morphology is formed by rods, while the γ-Ag_2WO_4 is formed by octahedrons, both in micrometer scale and with well-defined morphology. The photocatalytic tests indicate that the γ-Ag_2WO_4 phase has better photocatalytic activity compared to the β-Ag_2WO_4 phase. The scavenger's methodology indicated that h^+ charges are the main mechanism in the photocatalysis of methylene blue dye.

1. Introduction

Metal tungstates have been widely studied due to their wide range of applications such as photocatalysts, photoluminescence, batteries, sensors, antimicrobial agents, among others [1–5]. Moreover, the complexity of its structure compared to simple oxides allows greater control of its properties [4]. Among these tungstates, silver tungstate (Ag_2WO_4) has been gaining more attention due to the ease of being reduced metallic silver on its surface, favoring the generation of plasmon effect [6].

Silver tungstate has polymorphic characteristics, it can form in three distinct phases: α-Ag_2WO_4 (orthorhombic), β-Ag_2WO_4 (hexagonal) and γ-Ag_2WO_4 (cubic), where only the α-Ag_2WO_4 phase is stable under normal conditions. The β-Ag_2WO_4 and γ-Ag_2WO_4 phases being metastable [7,8]. Studies about the α-Ag_2WO_4 phase are easily found in the literature [9]. Studies on morphological alterations, as well as lattice modification or decorations to extend its properties, are found [10–12]. Senthil et al. [13] showed that the photocatalytic activity of α-Ag_2WO_4 can be optimized by the formation of heterostructure with AgBr nanoparticles. On the other hand, metastable phases have recently begun to gain attention. The main means of stabilization of the metastable phases are the use of surfactants, pH control and synthesis temperature [14–16]. Alvarez Roca et al. [8] synthesized the β-Ag_2WO_4 phase by precipitation for 20 min, controlling the reaction pH between 7 and 8, and showed the formation of silver nanoparticles on their surface through controlled electron irradiation. While Yin et al. [17] obtained β-Ag_2WO_4 particles without controlling the reaction pH, but using longer stirring times (6 h).

The γ-Ag_2WO_4 phase lacks studies regarding its obtaining and, mainly, characterization of its properties. Roca et al. [18] reported the synthesis of the γ-Ag_2WO_4 pure phase by a precipitation method using low temperature (5 °C) and short synthesis time (20 min), complementing the results with a DFT theoretical study. Thus, aiming to obtain this metastable phase γ-Ag_2WO_4 without the need for temperature control, the effect of the amount of PVP (nonionic surfactant) on the co-precipitation method at room temperature was studied. In addition, tests were conducted on the adsorptive and photocatalytic capacity against the methylene blue dye (cationic) and the scavenger's methodology was applied to determine the principles that act in photocatalysis.

* Corresponding author.
E-mail addresses: nfandraden@gmail.com, netoandrade@ufrn.edu.br (N.F. Andrade Neto).

https://doi.org/10.1016/j.ceramint.2020.03.012
Received 23 January 2020; Received in revised form 28 February 2020; Accepted 2 March 2020
Available online 03 March 2020

2. Materials and methods

2.1. Synthesis

Silver nitrate ($AgNO_3$ - Synth, 99%), sodium tungstate ($Na_2WO_4 \cdot 2H_2O$ - Synth, 99.5%), polyvinylpyrrolidone (PVP - $(C_6H_9NO)_n$ - Vetec P.M. 40.000), ammonium hydroxide (NH_4OH – Synth, 30%) and deionized water were used as precursor materials.

First, 4 mmol of silver nitrate was kept under magnetic stirring in 40 mL of deionized water until complete solubilization. Then, ammonium hydroxide was used to set the pH to 10, forming the solution (I). Simultaneously, a solution containing 2 mmol sodium tungstate and 40 mL deionized water was prepared, forming the solution (II). In both solutions PVP was added in the amounts of 0, 0.1, 0.3, 0.5 and 0.7 g. The solutions were stirred for 15 min to ensure complete dissolution and then the solution (I) containing the Ag^+ ions was quickly immersed in the solution (II) containing the W^{6+} ions and stirred for 30 min at room temperature, forming the final solution (III) at pH 7. The supernatant was then separated by centrifugation, washed with deionized water and dried at 60 °C for 24 h. After this period, the material was macerated. Fig. S1 (*supplementary materials*) shows the scheme of the synthesis. The samples were named according to the amount of PVP used in the synthesis: WS (without surfactant) and 0.1PVP, 0.3PVP, 0.5PVP and 0.7PVP referring to the quantities of 0.1, 0.3, 0.5 and 0.7 g of PVP, respectively.

2.2. Characterization

The powders were characterized by X-ray diffraction (Shimadzu, XRD-6000) using CuKα radiation (1.5418 Å), the powders were scanned from 10 to 60° using the speed of 1°/min and step of 0.01°. Rietveld refinement using the General Structure Analysis System (GSAS) program with graphical interface EXPGUI [19]. The Raman scattering spectra were recorded at room temperature with a resolution of 4 cm^{-1} and 64 scans, using a VERTEX 70 RAMII Bruker spectrophotometer (USA) with a Nd:YAG laser (1064 nm) and the maximum output power kept at 100 mW. A scanning electron microscope (SEM) was performed in a Hitachi tabletop microscope (model TM-3000) to observe the morphology of the Ag_2WO_4 phases. Transmission electron microscopy (TEM) and high-resolution transmission electron microscopy (HRTEM) was performed in FEI TECNAI G2 F20 microscope operating at 200 kV. The UV–Vis spectroscopy was performed on a Shimadzu UV-2550 equipment, with a wavelength range of 200–900 nm and programmed for the diffuse reflectance mode. Kubelka-Munk function [20] was applied to convert reflectance data in absorbance and Wood and Tauc methodology [21] was used to the energy of the bandgap (Egap) estimation.

2.3. Photocatalytic properties

The photocatalytic activity was estimated against the cationic methylene blue (MB) dye, at pH 5.0.05 g of the catalysts were placed in contact with 50 mL of the aqueous solution of MB (10^{-5} mol L^{-1} concentration) and kept under stirring for 30 min and an aliquot was taken every 10 min for analysis of adsorbent effects. After that time, six UVC lamps (TUV Philips, 15 W) illuminated the solutions for 60 min. The photocatalytic activity was then determined by the variation of the dyes absorption bands in Shimadzu UV-2600 spectrophotometer.

The mechanism acting on the photocatalytic process was determined by the use of charge, electron (e^-) and hole (h^+), and hydroxyl radical (·OH) sequestrants. For this, isopropyl alcohol (1 mL alcohol/100 mL dye), EDTA (7.2 mg EDTA/100 mL dye) and $AgNO_3$ (8.5 mg $AgNO_3$/100 mL dye) were used to suppress the action of hydroxyl radicals (·OH), positive charges (h^+) and negative charges (e^-), respectively.

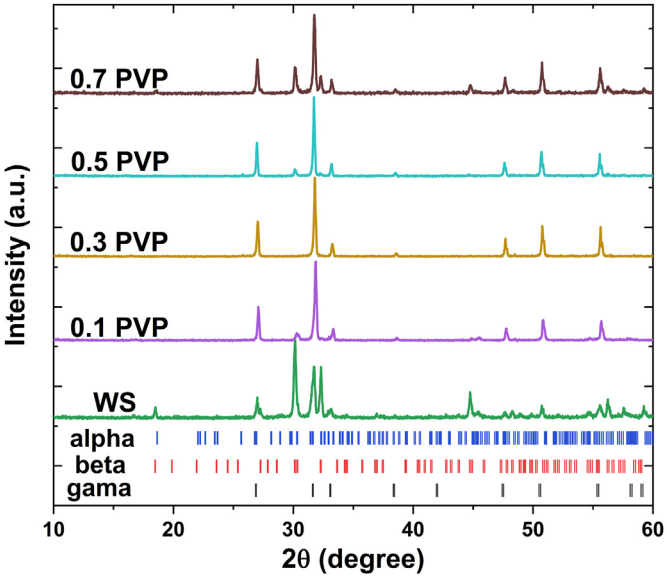

Fig. 1. Diffractograms obtained for the samples synthesized in this study with different amounts of PVP.

3. Results and discussion

Fig. 1 shows the diffractograms obtained for the materials synthesized in this work by varying the concentration of PVP. For synthesis without surfactant, there is the presence of the α-Ag_2WO_4 and β-Ag_2WO_4 phases. Previous work [1] showed that synthesis without the addition of ammonium hydroxide favors the formation of only α-Ag_2WO_4 stable phase, which does not occur for this synthesis at the final reaction pH 10. As PVP is inserted into the synthesis, the γ-Ag_2WO_4 phase stabilizes to 0.3PVP. Amounts greater than 0.3 g of PVP gradually destabilizes the γ-Ag_2WO_4 phase. For quantities greater than 0.7 g of PVP, no significant differences in metastable phase stabilization were observed, Fig. S2 (*supplementary material*) shows the diffractogram for the sample obtained using 2 g of PVP, being very similar to the sample obtained with 0.7 g. Thus, the study was restricted to quantities of up to 0.7 g of PVP. The α-Ag_2WO_4 phase has an orthorhombic crystalline system with space group Pn2n (no. 34), characterized by the ICSD card 243987 and β-Ag_2WO_4 phase has a hexagonal crystalline system with space group P6 (no. 168), characterized by the ICSD card 857465. While the γ-Ag_2WO_4 phase has a cubic crystalline system of space group Fd-3m (no. 227), characterized by ICSD card 864459.

As previously mentioned, the α-Ag_2WO_4 phase obtained by the coprecipitation method is stable for neutral/acid reaction media, while the shift to basic medium favors the appearance of metastable phases [17]. As indicated in the diffractograms, the use of PVP, nonionic surfactant, favors the stabilization of the γ-Ag_2WO_4 phase, obtaining an optimal ratio by adding 0.3 g of surfactant to the synthesis. PVP molecules interact with crystalline growth plans (111), favoring equivalent growth in all directions so that the γ-Ag_2WO_4 phase cubic structure is expected. The use of surfactants, whether ionic or nonionic, is widely studied due to their interaction with the crystalline growth planes, favoring the desired phase or morphology [22–24].

The Rietveld refinement was performed using GSAS software with the EXPGUI interface in all samples, to quantify the present phases and estimate the crystallite size and microstrain. For this, the refinement was performed using scale factor, phase fraction, Chebyshev polynomial function for background, Thomson-Cox-Hastingpseudo-Voigt peak format, changes in lattice parameters, atomic fraction coordinates and isotropic thermal parameters as parameters. Fig. 2 presents the curves obtained for the Rietveld refinement, illustrating the difference between theoretical (obs) and practical (calc) curves. The small

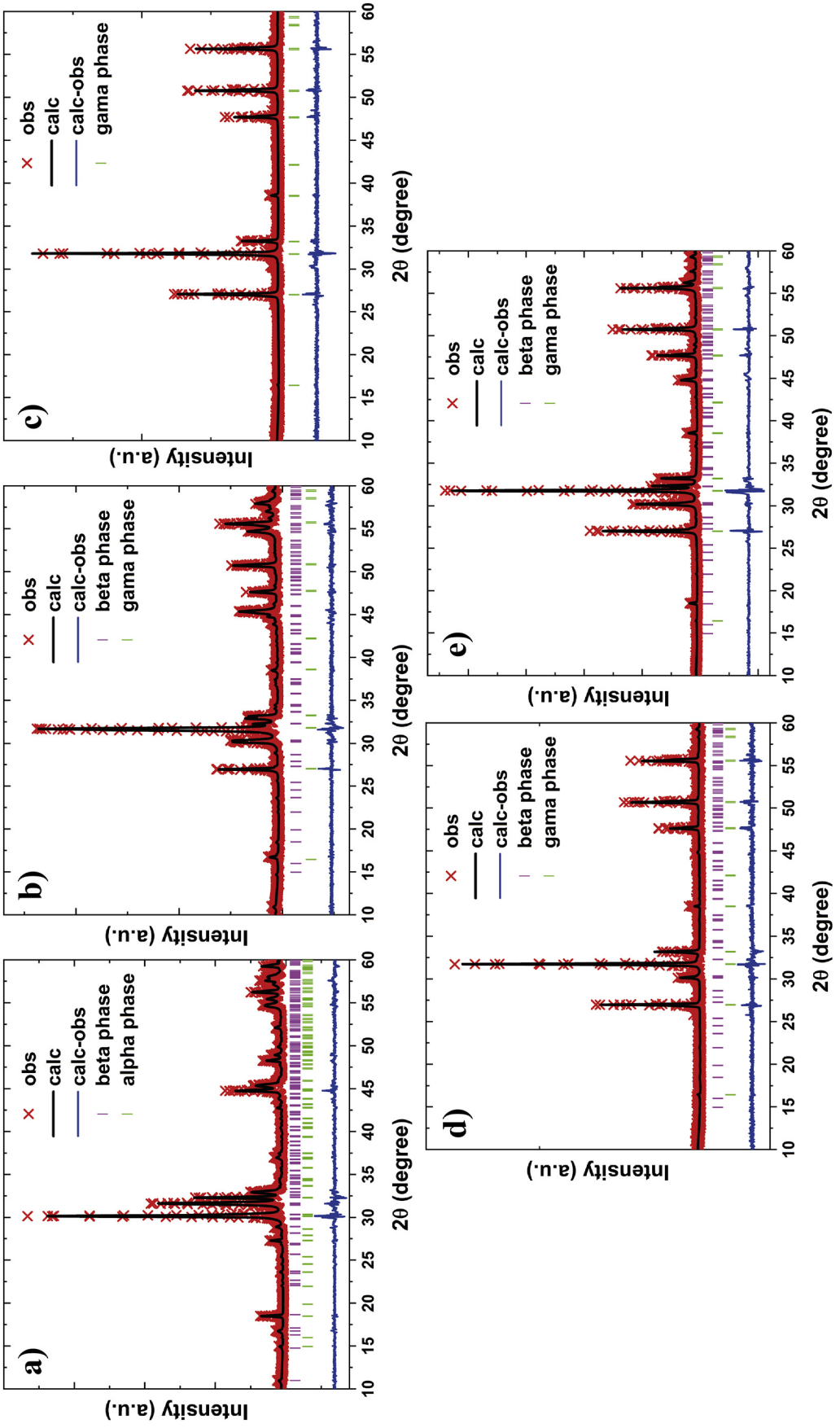

Fig. 2. Rietveld refinement for the Ag_2WO_4 samples.

Table 1
Microstructural parameters obtained by Rietveld refinement.

Samples		Crystallite size (nm)	Microstrain (10^{-3})	Phase (%)
WS	β	38.27	2.35	65.86
	α	30.08	3.14	34.14
0.1 PVP	β	22.71	3.98	17.63
	γ	42.56	2.26	82.37
0.3 PVP	γ	47.63	1.99	100
0.5 PVP	β	35.02	2.58	7.50
	γ	46.50	2.04	92.50
0.7 PVP	β	35.49	2.54	20.92
	γ	42.75	2.22	79.08

Table 2
Adjustment parameters of the Rietveld refinement.

	WS	0.1 PVP	0.3 PVP	0.5 PVP	0.7 PVP
w_{rp}	11.87	11.75	10.11	12.42	15.16
r_p	9.16	8.85	9.54	9.89	11.41
Chi^2	1.91	1.49	1.26	1.59	1.91
$R(F)^2$	6.36	4.76	4.41	8.31	9.52

difference between curves, associated with the low values of refinement constants, indicates the high quality of refinement, providing reliable data. Table 1 presents the microstructural values obtained through refinement and Table 2 shows de refinement parameters obtained by Rietveld refinement. According to the results shown, it is confirmed that the insertion of PVP in the synthesis, up to 0.3 g, provides the stabilization of the γ-Ag_2WO_4 phase, characterized by increased crystallite size and reduced crystallite size relative to the phase. β-Ag_2WO_4. As the amount of PVP is increased to 0.5 and 0.7 g, the γ-Ag_2WO_4 phase destabilization occurs.

Fig. 3 shows the Raman scattering spectra obtained with scanning from 100 to 1200 cm^{-1}. According to the spectra, there are scattering bands at 914, 882, 300 and 288 cm^{-1}. The 882 cm^{-1} band refers to the antisymmetrical elongation $\nu 3$ between W-O present in the [WO_4] cluster, while the 914 cm^{-1} band refers to the symmetrical elongation $\nu 1$. The 882 cm^{-1} band may still be associated with the symmetric stretching vibration of the W-O bond in [WO_6] octahedron cluster [25]. A comparison between intensities in the WS and 0.3PVP samples indicate that symmetrical elongation is more evident for the γ-Ag_2WO_4 phase, while the asymmetric elongation is β-Ag_2WO_4. On the other hand, the bands at 288 and 300 cm^{-1} correspond to symmetrical

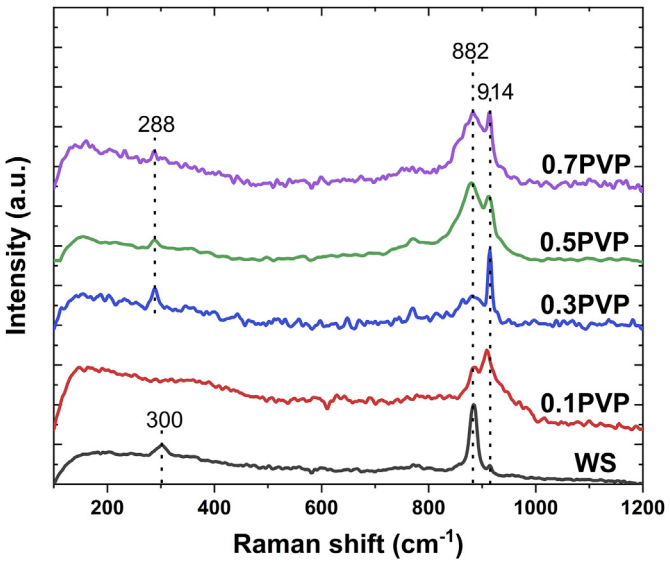

Fig. 3. Raman spectra for the samples obtained at different amounts of PVP.

elongation $\nu 2$ between O-W-O [26]. The displacement of the symmetrical elongation $\nu 2$ from 300 to 288 cm^{-1} is associated with the change of the crystal structure regarding the transition from the β-Ag_2WO_4 to γ-Ag_2WO_4 phase. In all curves is still visible the appearance of fluorescence at the beginning of the curves, coming from metallic silver [27]. The relationship between Raman intensities for elongations $\nu 1$ and $\nu 3$ is consistent with the quantifications of the phases present in diffractograms, shown earlier in Fig. 1.

Fig. 4 shows SEM images for Ag_2WO_4 particles obtained at different amounts of PVP. According to Fig. 4a, the particles obtained without PVP have a brittle aspect, with some incomplete rods. Thus, it can be assumed that increasing the pH in parallel to the absence of PVP prevents the growth of well-defined rods morphology particles. As reported in the literature, the α-Ag_2WO_4 and β-Ag_2WO_4 phases grow preferentially in the form of dense rods in the micrometer scale [8,25]. The growth of particles to form a well-defined surface morphology is directly related to the energy of each crystal surface. Roca et al. [28] showed the influence of the crystalline plane energy on the formation of specific morphology through DFT theoretical calculations, being favorable the growth on the lower energy planes. The formation of the rods related to the β-Ag_2WO_4 phase occurs due to the influence of the planes (011) and (110), being more influenced by the latter. On the other hand, according to the theoretical data reported in another study by Roca et al. [18], the preferential growth in (111) plane favors the formation of octahedral particles, with balloon-like morphology, characteristic of the γ-Ag_2WO_4 phase, as can be seen in Fig. 4c, being the only morphology present.

Thus, the use of PVP as a surfactant tends to favor growth in-plane (111) for up to 0.3 g. Increasing the amount of PVP during the synthesis favors the growth in the (011) and (110) planes to the amount of 0.7 g. Quantities greater than 0.7 g do not promote significant changes in the formation of different phases and morphology. Fig. 5 illustrates the growth plans for the β-Ag_2WO_4 and γ-Ag_2WO_4 crystals. The surfactants are formed by molecules that can be divided into two parts, polar (hydrophobic) and nonpolar (hydrophilic), where their use in small amounts favors the adsorption in the surface of growth planes of the materials, reducing their surface tension and favoring the growth at well-defined morphologies [29]. On the other hand, the use of high amounts of surfactant provides greater interaction between its functional groups, favoring the micelle formation, rather than acting primarily on the surface energy of growth plans [30]. The use of PVP increases the viscosity of the solution as concentration increases, inducing a steric effect on crystalline growth and preventing transformation to the stable phase α-Ag_2WO_4 [31,32].

Fig. 6 shows the TEM and HRTEM images for the 0.3PVP sample. According to the image, the growth of metallic silver on the octahedron surface can be seen, as shown in Fig. 6a–c. TEM images confirm that the particles are dense, not allowing the viewing of the diffraction planes. The silver particle grown on the surface does not allow visualization of the diffraction plane due to its constant growth due to the high power of the incident beam. Fig. 6b illustrates the appearance of several Ag^0 nanoparticles on the surface of Ag_2WO_4 and Fig. 6c confirms their growth with beam permanence. Spot EDX analysis was performed on the grown particle as indicated in red, confirming that it was Ag^0. These nanoparticles act by producing the surface plasmon effect (SPE), increasing the capacity of electron capture and storage [16]. Thus, the electrons present in the conduction band of Ag_2WO_4 migrate to the Ag^0 nanoparticles on their surface, acting as a charge separator. Finally, these electrons (e^-) in the conduction band act as reducing centers, while the holes (h^+) present in the valence band act as oxidation centers.

Diffuse reflectance spectroscopy was performed on Ag_2WO_4 powders and the data obtained were converted for absorption by the Kubelka-Munk methodology. The equation proposed by Wood and Tauc was then applied using the allowed direct transition to estimate the gap band energy (Egap) of the powders. Fig. 7a shows the absorption curves

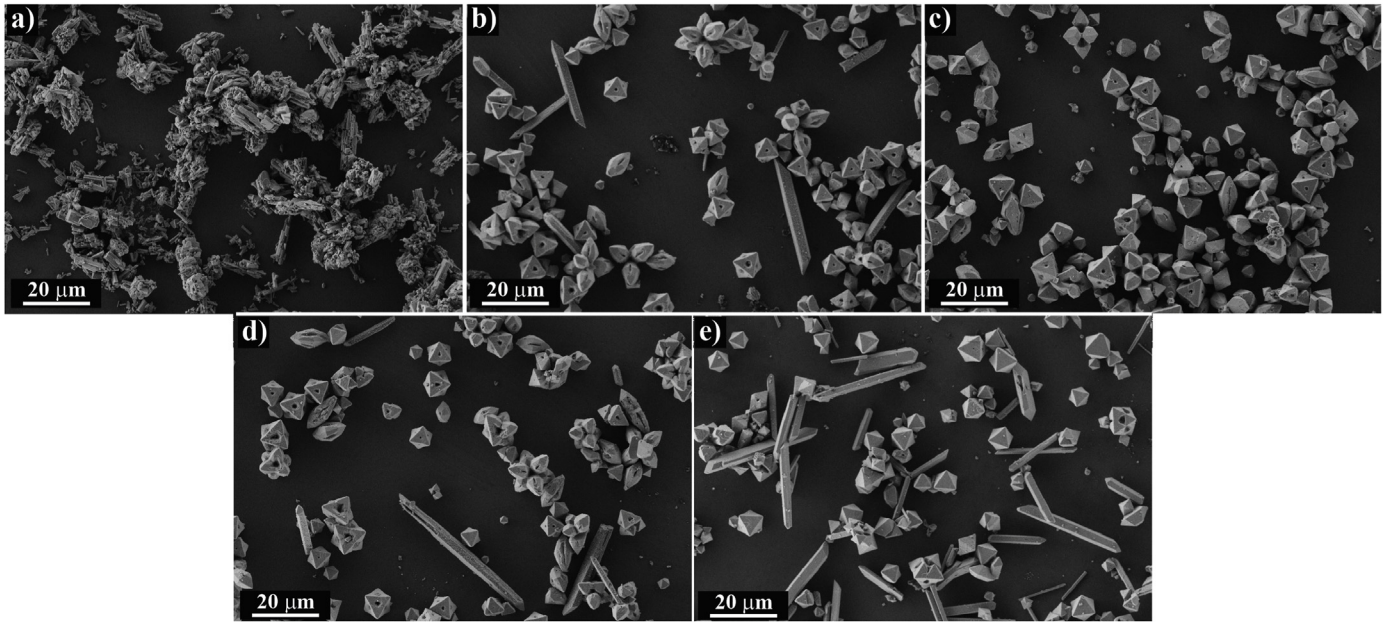

Fig. 4. SEM images for (a) without PVP, (b) 0.1PVP, (c) 0.3PVP, (d) 0.5PVP and (e) 0.7PVP samples.

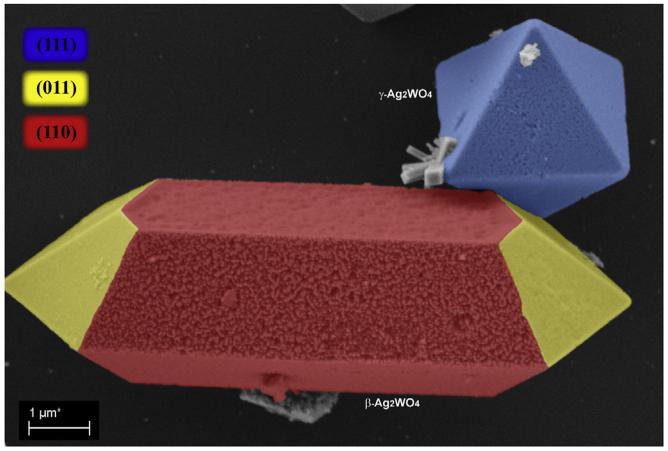

Fig. 5. SEM images illustrating the plans present in the grown-up crystal for the 0.1PVP sample.

obtained for the Ag_2WO_4 powders and the curves shown in Fig. 7b–f illustrates the Egap obtained by the allowed direct transition (α^2). According to Fig. 7a, WS and 0.1PVP samples show higher absorption around 347 nm, as the amount of PVP increases, the maximum absorption shifts to shorter wavelengths in around 311 nm, this absorption being more evident for the 0.3PVP sample, which presents only the γ-Ag_2WO_4 phase. All samples have an absorption band near 227 nm. As shown in the diffractograms, WS and 0.1PVP samples show a higher β-Ag_2WO_4 phase percentage. The absence of absorption at 347 nm for the sample containing only the γ-Ag_2WO_4 phase, in parallel with the increase in absorption for the WS sample, allows us to attribute this absorption to the β-Ag_2WO_4 phase. This increase in absorption for longer wavelengths is best seen through the obtained Egap, where the samples with the largest amount of the γ-Ag_2WO_4 phase have the highest Egap, being 3.54, 3.53, 3.49, 3.18 and 3.23 eV for the samples. 0.3PVP, 0.5PVP, 0.7PVP, 0.1PVP and WS. These results are according to literature reports [33,34].

The discoloration capacity of the powders obtained in this work was measured against the methylene blue (MB) dye, cationic, for 90 min, being 30 min without the presence of external radiation source, for consideration of the adsorptive effect and 60 min under UVC radiation, for analysis of photocatalytic effect. Fig. 8 shows the concentration curves of the MB dye variation by the test time. Adsorption tests are not directly related to the amount of phase present. As highlighted in Fig. 8, complete discoloration occurs after 70 min for the samples containing 0.3 and 0.5 g PVP, corresponding to the sample containing only the γ-Ag_2WO_4 phase and the sample containing 7.5% of the β-Ag_2WO_4 phase, respectively. As the amount of the β-Ag_2WO_4 phase increases, the MB discoloration decreases, where the WS sample, which has the largest amount, has the worst result. Thus, it can be assumed that the γ-Ag_2WO_4 phase has better photocatalytic activity than the β-Ag_2WO_4 phase. After the photocatalytic test, XRD analysis was performed on the powder, as shown in Fig. S3 (*supplementary material*), the non-formation of secondary phases indicates the stability of the material.

As proposed by Roca et al. [18], the (111) plane has bigger energy compared to other specifics growth surfaces for the γ-Ag_2WO_4. This high energy is associated with more electrons in your surface, contributing to the photocatalytic process. On the other hand, in your other work, Roca et al. [28] showed that the (110) and (011) planes have the lowest energy compared to the other planes for the β-Ag_2WO_4, reducing the electrons in your surface. Furthermore, the Egap of the γ-Ag_2WO_4 phase can be attributed to the (111) plane, while the Egap for the β-Ag_2WO_4 phase is related to the two growth (110) and (001) plans. The greater Egap of the γ-Ag_2WO_4 phase generates a greater energy barrier, making it difficult to recombine the photogenerated electron/hole (e^-/h^+) pairs during the photocatalytic process, compared to the other phases. The non-recombination of the e^-/h^+ pairs allows their action in the degradation of the MB dye.

Further information regarding the photocatalytic mechanism of γ-Ag_2WO_4 particles obtained with 0.3 g PVP was obtained by applying the charge scavenger methodology, which adds specific chemical reagents to the dye and photocatalyst solution to isolate the acting mechanisms. Fig. 9 shows curves of the methylene blue (MB) dye concentration comparing the solution without scavenger (WS) with solutions containing silver nitrate (AgNO), Ethylenediaminetetraacetic acid (EDTA) and isopropyl alcohol (IA). According to these curves, the scavengers reduce the adsorption capacity of the 0.3PVP sample, this reduction is most evident for the solution containing silver nitrate. In contrast, this solution presented better photocatalytic results, superior even the solution without scavenger. Silver nitrate in the solution acts to capture available electrons, thereby removing negative charges (e^-)

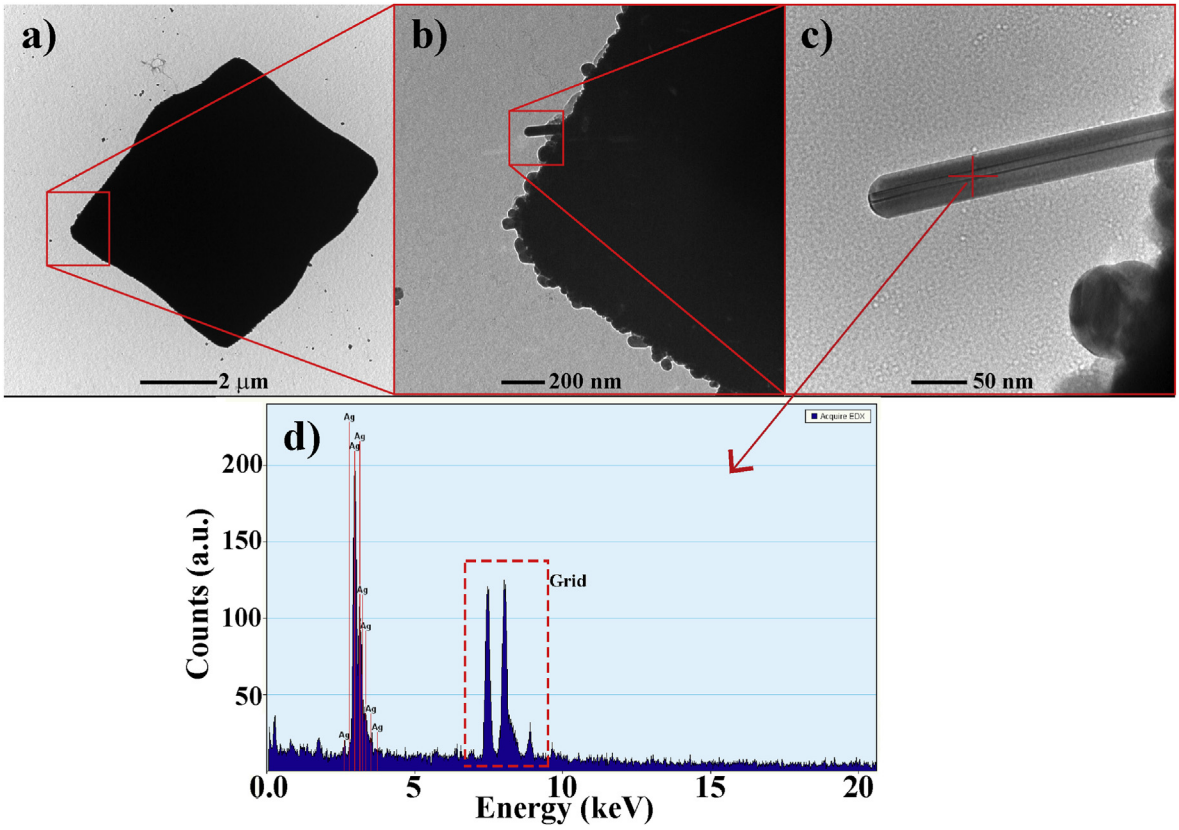

Fig. 6. (a)-(b) TEM and (c) HRTEM images for the 0.3PVP sample and (d) EDX performed in nanorod of silver.

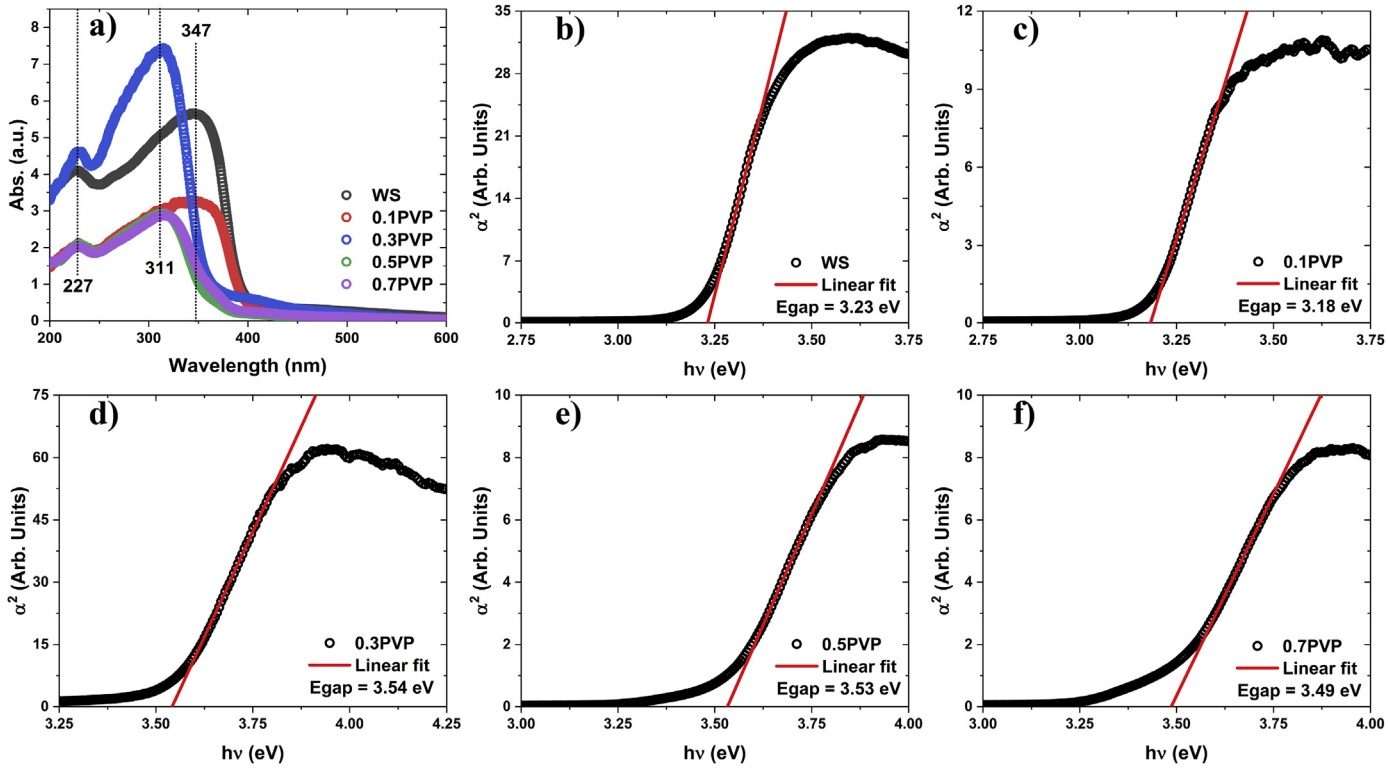

Fig. 7. (a) Absorption curves obtained by Kubelka-Munk function and extrapolation of the linear portion refer to permissible direct transition according to Wood and Tauc methodology for (b) WS, (c) 0.1PVP, (d) 0.3PVP, (e) 0.5PVP and (f) 0.7PVP.

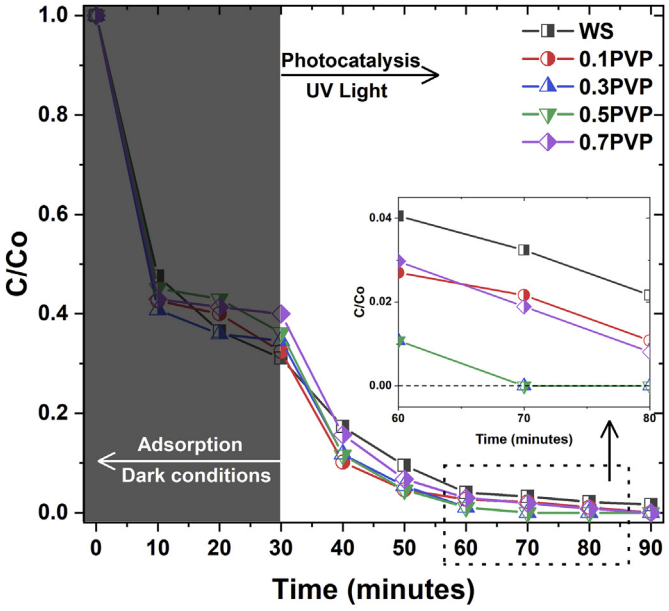

Fig. 8. Variation of the MB dye concentration versus test time for the samples obtained in this work.

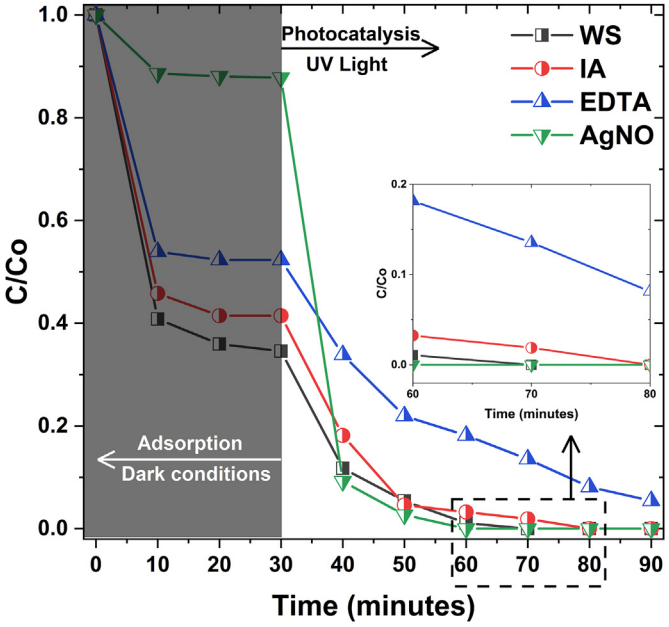

Fig. 9. Variation of the MB dye concentration *versus* test time for the 0.3PVP sample comparing different scavengers.

from the surface of the material responsible for the electrostatic attraction of the dye MB cationic molecules. On the other hand, electron restriction (e^-) causes photogenerated holes (h^+) to "lose" their recombination pair, remaining in the valence band and becoming available for the reduction reactions that produce H_2O_2 species with high oxidative power [35]. One of the basic principles of photocatalysis is in the generation and prevention of electron/hole (e^-/h^+) recombination, where the e^- free in the conduction band migrates to the material surface, producing reduction reactions, while the generated h^+ in the valence band migrate to the surface and produce oxidation reactions [36]. The use of EDTA and isopropyl alcohol reduced photocatalytic activity, this reduction is more evident for the EDTA solution. EDTA acts in opposition to silver nitrate, restricting the holes (h^+) and leaving only the electrons (e^-) available for catalytic reactions, while isopropyl alcohol inhibits the catalytic action of ·OH radicals. Thus, the photocatalytic activity of the γ-Ag_2WO_4 phase occurs mainly due to the oxidation reactions performed by the h^+ available in the valence band, which produce high oxidative capacity H_2O_2 against organic dyes. While the small reduction in photocatalytic capacity from inhibition of ·OH radicals indicates its low influence on the degradation of methylene blue dye. Fig. S4 (*supplementary materials*) shows a scheme of the disponible charges for act on photocatalysis in the γ-Ag_2WO_4 particles surface.

4. Conclusion

The use of PVP as a surfactant was efficient in stabilizing the γ-Ag_2WO_4 phase to 0.3 g, wherein larger or smaller amounts favored the formation of α-Ag_2WO_4 and β-Ag_2WO_4 as secondary phases. The basic reaction medium in parallel to the absence of PVP prevents the formation of particles with definite morphology, while the presence of PVP forms β-Ag_2WO_4 phase consisting of micrometer-scale rods, which grow preferentially in the planes (011) and (110), and the γ-Ag_2WO_4 phase forms octahedron that grows through the plane (111). All phases present absorption in the ultraviolet region. The photocatalytic tests show that the γ-Ag_2WO_4 phase has better results than the β-Ag_2WO_4 and α-Ag_2WO_4 phases in the degradation of methylene blue dye. The H_2O_2 species generated by the reduction reactions from h^+ form the main photocatalytic mechanism. The use of PVP was also efficient in maintaining the γ-Ag_2WO_4 phase, where even after photocatalytic tests under UVC radiation, the phase remains chemically stable.

Declaration of competing interests

The authors declare that they have no known competing financial interests or personal relationships that could have appeared to influence the work reported in this paper.

Acknowledgment

This study was partially financed in part by the Coordenação de Aperfeiçoamento de Pessoal de Nível Superior - Brasil (CAPES/PROCAD) - Finance Code 2013/2998/2014 and the author's thanks to the financial support of the Brazilian research financing institution (CNPq) No. 307546/2014 and São Paulo Research Foundation No. 2013/07296-2.

Appendix A. Supplementary data

Supplementary data to this article can be found online at https://doi.org/10.1016/j.ceramint.2020.03.012.

References

[1] N.F. Andrade Neto, P.M. Oliveira, M.R.D. Bomio, F.V. Motta, Effect of temperature on the morphology and optical properties of Ag2WO4 obtained by the co-precipitation method: photocatalytic activity, Ceram. Int. 45 (2019) 15205–15212.
[2] T. Peng, C. Liu, X. Hou, Z. Zhang, C. Wang, H. Yan, Y. Lu, X. Liu, Y. Luo, Control growth of mesoporous nickel tungstate nanofiber and its application as anode material for lithium-ion batteries, Electrochim. Acta 224 (2017) 460–467.
[3] S.K. Ganiger, B.V. Chaluvaraju, S.R. Ananda, M.V. Murugendrappa, A feasibility study of polypyrrole/zinc tungstate (ceramics) nano composites for D. C. Conductivity and as a humidity sensor, Mater. Today: Proc. 5 (2018) 2803–2810.
[4] F.X. Nobre, I.S. Bastos, R.O. dos Santos Fontenelle, E.A.A. Júnior, M.L. Takeno, L. Manzato, J.M.E. de Matos, P.P. Orlandi, J. de Fátima Souza Mendes, W.R. Brito, P.R. da Costa Couceiro, Antimicrobial properties of α-Ag2WO4 rod-like microcrystals synthesized by sonochemistry and sonochemistry followed by hydrothermal conventional method, Ultrason. Sonochem. 58 (2019) 104620.
[5] N.F.A. Neto, T.B.O. Nunes, M. Li, E. Longo, M.R.D. Bomio, F.V. Motta, Influence of microwave-assisted hydrothermal treatment time on the crystallinity, morphology and optical properties of ZnWO4 nanoparticles: photocatalytic activity, Ceram. Int. 46 (2020) 1766–1774.
[6] F.A. Sofi, K. Majid, Plasmon induced interfacial charge transfer across Zr-based metal-organic framework coupled Ag2WO4 heterojunction functionalized by Ag

NPs: efficient visible light photocatalyst, Chem. Phys. Lett. 720 (2019) 7–14.
[7] Q. Li, J. Yao, M. Arif, T. Huang, X. Liu, G. Duan, X. Yang, Facile fabrication and photocatalytic performance of WO3 nanoplates in situ decorated with Ag/β-Ag2WO4 nanoparticles, J. Environ. Chem. Eng. 6 (2018) 1969–1978.
[8] R. Alvarez Roca, P.S. Lemos, J. Andrés, E. Longo, Formation of Ag nanoparticles on metastable β-Ag2WO4 microcrystals induced by electron irradiation, Chem. Phys. Lett. 644 (2016) 68–72.
[9] Z. Zhu, F. Zhou, S. Zhan, Enhanced antifouling property of fluorocarbon resin coating (PEVE) by the modification of g-C3N4/Ag2WO4 composite step-scheme photocatalyst, Appl. Surf. Sci. 506 (2020) 144934.
[10] C. Ayappan, B. Palanivel, V. Jayaraman, T. Maiyalagan, A. Mani, One-step hydrothermal synthesis of CaWO4/α-Ag2WO4 heterojunction: an efficient photocatalyst for removal of organic contaminants, Mater. Sci. Semicond. Process. 104 (2019) 104693.
[11] Y. Fang, Y. Cao, Q. Chen, Synthesis of an Ag2WO4/Ti3C2 Schottky composite by electrostatic traction and its photocatalytic activity, Ceram. Int. 45 (17) (2019) 22298–22307.
[12] M. Pirhashemi, A. Habibi-Yangjeh, Preparation of novel nanocomposites by deposition of Ag2WO4 and AgI over ZnO particles: efficient plasmonic visible-light-driven photocatalysts through a cascade mechanism, Ceram. Int. 43 (2017) 13447–13460.
[13] R.A. Senthil, S. Osman, J. Pan, A. Khan, V. Yang, T.R. Kumar, Y. Sun, Y. Lin, X. Liu, A. Manikandan, One-pot preparation of AgBr/α-Ag2WO4 composite with superior photocatalytic activity under visible-light irradiation, Colloid. Surface. Physicochem. Eng. Aspect. 586 (2020) 124079.
[14] X. Wang, C. Fu, P. Wang, H. Yu, J. Yu, Hierarchically porous metastable β-Ag2WO4hollow nanospheres: controlled synthesis and high photocatalytic activity, Nanotechnology 24 (2013) 165602.
[15] F.P. Barrows, M.H. Bartl, Photonic structures in biology: a possible blueprint for nanotechnology, Nanomater. Nanotechnol. 4 (2014) 1.
[16] H. Chen, Y. Xu, Photoactivity and stability of Ag2WO4 for organic degradation in aqueous suspensions, Appl. Surf. Sci. 319 (2014) 319–323.
[17] H. Yin, M. Zhang, J. Yao, Y. Luo, P. Li, X. Liu, S. Chen, Surfactant-assisted synthesis of direct Z-scheme AgBr/β-Ag2WO4 heterostructures with enhanced visible-light-driven photocatalytic activities, Mater. Sci. Semicond. Process. 105 (2020) 104688.
[18] R.A. Roca, P.S. Lemos, L. Gracia, J. Andrés, E. Longo, Uncovering the metastable γ-Ag2WO4 phase: a joint experimental and theoretical study, RSC Adv. 7 (2017) 5610–5620.
[19] B. Toby, EXPGUI, a graphical user interface for GSAS, J. Appl. Crystallogr. 34 (2001) 210–213.
[20] M. Patel, A. Chavda, I. Mukhopadhyay, J. Kim, A. Ray, Nanostructured SnS with Inherent Anisotropic Optical Properties for High Photoactivity, (2015).
[21] B.D. Viezbicke, S. Patel, B.E. Davis, D.P. Birnie Iii, Evaluation of the Tauc method for optical absorption edge determination: ZnO thin films as a model system, Phys. Status Solidi 252 (2015) 1700–1710.
[22] M. Chakraborty, F.-W. Hsiao, B. Naskar, C.-H. Chang, A.K. Panda, Surfactant-Assisted synthesis and characterization of stable silver bromide nanoparticles in aqueous media, Langmuir 28 (2012) 7282–7290.
[23] Y.D. Li, X.L. Li, R.R. He, J. Zhu, Z.X. Deng, Artificial lamellar mesostructures to WS 2 nanotubes, J. Am. Chem. Soc. 124 (2002) 1411–1416.
[24] H. Jiang, H. Dai, X. Meng, K. Ji, L. Zhang, J. Deng, Porous olive-like BiVO4: alcohohydrothermal preparation and excellent visible-light-driven photocatalytic performance for the degradation of phenol, Appl. Catal. B Environ. 105 (2011) 326–334.
[25] C. Ayappan, V. Jayaraman, B. Palanivel, A. Pandikumar, A. Mani, Facile preparation of novel Sb2S3 nanoparticles/rod-like α-Ag2WO4 heterojunction photocatalysts: continuous modulation of band structure towards the efficient removal of organic contaminants, Separ. Purif. Technol. 236 (2020) 116302.
[26] D. Kumar, B.P. Singh, M. Srivastava, A. Srivastava, P. singh, A. Srivastava, S.K. Srivastava, Structural and photoluminescence properties of thermally stable Eu3 + activated CaWO4 nanophosphor via Li + incorporation, J. Lumin. 203 (2018) 507–514.
[27] N.F. Andrade Neto, Y.G. Oliveira, J.H.O. Nascimento, B.R. Carvalho, M.R.D. Bomio, F.V. Motta, Synthesis, characterization, optical properties investigation and reusability photocatalyst capacity of AgCl-xGO composite, J. Mater. Sci. Mater. Electron. 30 (2019) 15214–15223.
[28] R.A. Roca, A.F. Gouveia, P.S. Lemos, L. Gracia, J. Andrés, E. Longo, formation of Ag nanoparticles on β-Ag2WO4 through electron beam irradiation: a synergetic computational and experimental study, Inorg. Chem. 55 (2016) 8661–8671.
[29] B. Thiele, K. Günther, M.J. Schwuger, Alkylphenol ethoxylates: trace analysis and environmental behavior, Chem. Rev. 97 (1997) 3247–3272.
[30] N. Scholz, T. Behnke, U. Resch-Genger, Determination of the critical micelle concentration of neutral and ionic surfactants with fluorometry, conductometry, and surface tension—a method comparison, J. Fluoresc. 28 (2018) 465–476.
[31] S.-M. Lam, M.-W. Kee, J.-C. Sin, Influence of PVP surfactant on the morphology and properties of ZnO micro/nanoflowers for dye mixtures and textile wastewater degradation, Mater. Chem. Phys. 212 (2018) 35–43.
[32] M. Ren, J. Song, Y. Shi, Y. Xiang, G. Hu, Synthesis of zinc pyrovanadate 3D flower-like microspheres and their photocatalytic properties, J. Cryst. Growth 402 (2014) 119–123.
[33] Y. Li, R. Jin, X. Fang, Y. Yang, M. Yang, X. Liu, Y. Xing, S. Song, In situ loading of Ag2WO4 on ultrathin g-C3N4 nanosheets with highly enhanced photocatalytic performance, J. Hazard Mater. 313 (2016) 219–228.
[34] P. Askari, S. Mohebbi, T.-O. Do, High performance plasmonic activation of Ag on β-Ag2WO4/BiVO4 as nanophotocatalyst for oxidation of alcohols by incident visible light, J. Photochem. Photobiol. Chem. 367 (2018) 56–65.
[35] N.F. Andrade Neto, K.N. Matsui, C.A. Paskocimas, M.R.D. Bomio, F.V. Motta, Study of the photocatalysis and increase of antimicrobial properties of Fe3 + and Pb2 + co-doped ZnO nanoparticles obtained by microwave-assisted hydrothermal method, Mater. Sci. Semicond. Process. 93 (2019) 123–133.
[36] N.F.A. Neto, L.M.P. Garcia, E. Longo, M.S. Li, C.A. Paskocimas, M.R.D. Bomio, F.V. Motta, Photoluminescence and photocatalytic properties of Ag/AgCl synthesized by sonochemistry: statistical experimental design, J. Mater. Sci. Mater. Electron. 28 (2017) 12273–12281.